JOURNAL OF SPACECRAFT AND ROCKETS
Vol. 31, No. 1, January–February 1994

Effects of the Roll Angle on Cruciform Wing-Body Configurations at High Incidences

J. Meyer*
Technion—Israel Institute of Technology, Haifa, Israel

Three cruciform wings were tested on a body at five roll angles and up to three longitudinal positions in a low-speed wind tunnel, up to an angle of attack of $\alpha = 90$ deg. The roll angle affects significantly the fin normal force coefficient. The normal force on the upper fins decreases to zero, at $\alpha > 40$ deg, possibly because the vortex breakdown on the lower fins induces separated flow over the upper fins. As a consequence, a strong rolling moment is induced at these incidences at asymmetric roll angles. This rolling moment is independent of the wing axial position but proportional to the wing planform area, similarly to the fin normal force coefficient. This rolling moment is much larger than the rolling moment induced on symmetrical configurations by the asymmetric body vortices. The wing contribution to the side force is small compared with the body contribution at asymmetric roll angles. As a result, the maximum side force is not higher than that obtained at symmetric + and × attitudes.

Nomenclature

C_N = normal force coefficient, based on area S_{ref}
C_{N_F} = fin normal force coefficient, based on area S_{ref}
$C_{N_F}^*$ = fin normal force coefficient, based on area S^*
C_n = yawing moment coefficient, based on area S_{ref} and diameter d
C_R = rolling moment coefficient, based on area S_{ref} and diameter d
C_R^* = rolling moment coefficient, based on area S^* and diameter d
C_Y = side force coefficient, based on area S_{ref}
d = body diameter; reference length for moment coefficients, m
Re_d = Reynolds number, based on diameter d
S_{ref} = body maximal cross section; reference area for force and moment coefficients, unless otherwise defined, m^2
S_W = planform area of one pair of joined wings, m^2
S^* = one fin planform area; reference area for $C_{N_F}^*$ and C_R^*, m^2
X_{cp_F} = fin longitudinal center of pressure, measured from the fin root chord apex, m
X_{cp} = main normal force center of pressure, measured backward from the moment reference center, at $4.5d$ from the body nose, m
Y_{cp_F} = fin lateral center of pressure, measured from the root chord, m
α = model angle of attack, deg
θ = azimuthal angle, measured clockwise from the windward edge of the body when looking forward, cf. Fig. 1, deg
ϕ = model roll angle, positive clockwise when looking forward, zero at + attitude, cf. Fig. 1, deg

Subscripts
B = value of a coefficient for the body alone
$B(W)$ = body contribution to a coefficient
$W(B)$ = wing contribution to a coefficient

Introduction

An increasing number of aircraft and missiles fly at high incidences either to develop high lift or because of imposed flight trajectory. Such a case may be found for vertical launch vehicles, where high angles of attack are reached during the launch phase.[1] In such a trajectory, arbitrary roll angles may be encountered, due to wind velocity or arbitrary target azimuth. A combination of high angles of attack and asymmetrical roll angles produces high lateral aerodynamic coefficients, such as side force, yawing moment, and rolling moment.

Many studies have been conducted on high-incidence characteristics for bodies, wings, or symmetrical wing-body combinations, giving details on the vortex lift, the vortex breakdown, and interactions between wing and body vortices.[2–4] Many studies have also been conducted on out-of-plane or lateral aerodynamic characteristics for symmetrical configurations, giving details about asymmetric vortices developed on bodies[5–8] and proposing methods for reducing them.[9–12]

However, much less has been reported about asymmetric loads on configurations at asymmetrical roll angles. For such configurations, some of these forces are not due to asymmetrical vortices shed along the body but are induced by deterministic loads, resulting from flow separation on some of the fins.

The purpose of this work is to analyze the aerodynamic coefficients of wing-body configurations, especially asymmetric loads at asymmetric roll angles. For this objective, three cruciform wings were tested on a body at five roll angles and up to three longitudinal positions. In that way, the effect of the roll angle, together with the influence of the wing area and position, was analyzed.

Experimental Installation

The tests were conducted at the Technion 1×1 m low-speed wind tunnel at a Mach number of 0.1 and a Reynolds number of $Re_d = 1 \times 10^5$ at incidences up to $\alpha = 90$ deg.

The model, of diameter $d = 0.046$ m, had a pointed tangent ogive nose of fineness ratio 2, a circular cylindrical afterbody, and a total length of $10d$; see Fig. 1. Three cruciform wings—A, B, and C—were added to the body. They had the same exposed semispan ($1.5d$), the same leading-edge sweep angle (63.4 deg), and no trailing-edge sweep. Their taper ratios were 0, 0.14, and 0.25, respectively; their exposed surfaces (i.e., the surface of one pair of fin panels joined at their root chord) were $S_W = 4.5d^2$, $6d^2$, and $7.5d^2$, respectively; and their exposed aspect ratios were 2, 1.5, and 1.2, respectively. The thickness of the wings was 3 mm. The wings' leading edge, side edge, and trailing edge had a bevelled shape with an angle of 10 deg.

The wings were added to the body with their apex at the same position ($4.5d$ from the body nose, referred to as the midposition). Wing B was also set up with its apex at $2.4d$ from the body nose (fore position) and at $6.0d$ from it (back position). The moment reference center was located at $4.5d$ from the body nose for all wing positions. No transition trips were used in these tests; there-

Presented as Paper 92-4356 at the AIAA Atmospheric Flight Mechanics Conference, Hilton Head, SC, Aug. 10–12, 1992; received Sept. 26, 1992; revision received Jan. 8, 1993; accepted for publication Jan. 11, 1993.

*Senior Lecturer, Faculty of Aerospace Engineering. Member AIAA.

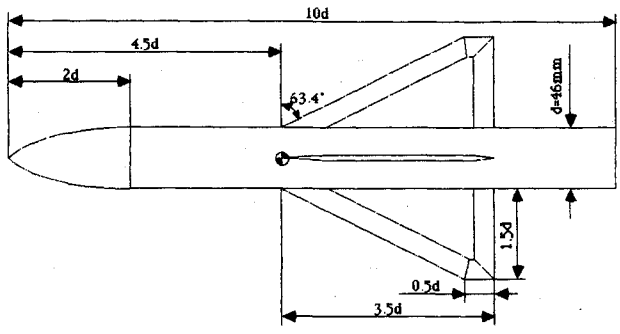

Wing B - Mid Position Configuration

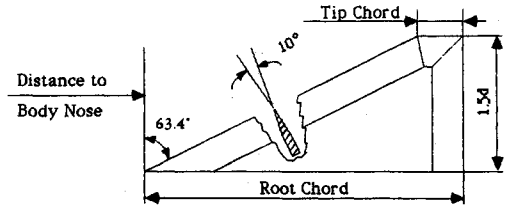

Configuration	Distance to Nose	Root Chord	Tip Chord
Wing A - Mid Position	4.5d	3.0d	0.
Wing B - Fore Position	2.4d	3.5d	0.5d
Wing B - Mid Position	4.5d	3.5d	0.5d
Wing B - Back Position	6.0d	3.5d	0.5d
Wing C - Mid Position	4.5d	4.0d	1.0d

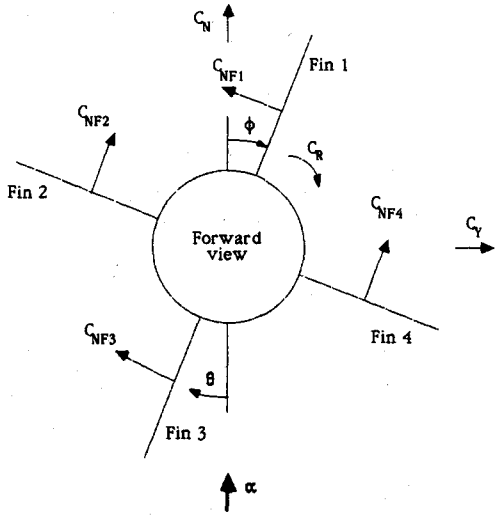

Fig. 1 Details of the model.

fore the boundary layer is expected to be mainly laminar at high incidences, where symmetric or asymmetric vortices are shed from the body.

These wing-body configurations were tested at five roll angles: $\phi = 0$, 11, 22.5, 34, and 45 deg, where $\phi = 0$ deg refers to the "+" attitude, ϕ being positive clockwise when looking forward; see Fig. 1. At the + attitude, fin 1 is the vertical fin on the lee side of the body, and fins 2 and 4 are horizontal, fin 2 being at the left side, when looking forward. The circumferential position of each fin is denoted by the azimuthal angle θ, measured clockwise from the windward edge of the body when looking forward.

The model was mounted on a sting support, as shown in Fig. 2, which presents minimal interference at the high-angle-of-attack regime.[8] Aerodynamic forces and moments were measured by a main six-component internal strain-gauge sting balance, as well as secondary internal strain-gauge balances (measuring normal force, pitching, and bending moments) for each of the four fins. The aerodynamic coefficients were normalized by the body cross-sectional area S_{ref} and its diameter d, unless otherwise defined. Main coefficients refer to the unrolled body axis system, but the fin normal force coefficient C_{N_F} is always directed normal to the fin, as seen in Fig. 1. The accuracy of the main balance is 0.2, 0.15, 0.1, and 0.4 for the normal force coefficient C_N, the side force coefficient C_Y, the rolling moment coefficient C_R, and the yawing moment coefficient C_n, respectively, and 2% for the center of pressure X_{cp}. The accuracy of the secondary balances is 0.01 for C_{N_F} and 0.45 and 0.25% for the longitudinal and lateral centers of pressure X_{cp_F} and Y_{cp_F}, respectively.

Fin Loads

The fin normal force coefficient C_{N_F} is presented in Fig. 3 for the wing B at midposition and $\phi = 0$ deg (+ attitude). The normal force coefficient on the horizontal fins increases up to $\alpha \approx 35$ deg, where the wing vortex breakdown occurs, as reported[3] for a 65-deg-swept delta wing. At higher incidences, after some decrease as a result of the breakdown, C_{N_F} remains generally constant with α, as already reported for a flat plate at incidence.[13] Its center of pressure moves forward and inward at $\alpha < 20$ deg, as a result of the vortex lift on the fin, then backward at the vortex breakdown,[3] until it reaches the longitudinal planform area center at $\alpha = 90$ deg, as predicted by the crossflow theory.[14] The incidence range $\alpha < 35$ deg clearly corresponds to axially dominated flow, whereas the range $\alpha > 65$ deg corresponds to the crossflow prevailing at high incidences.

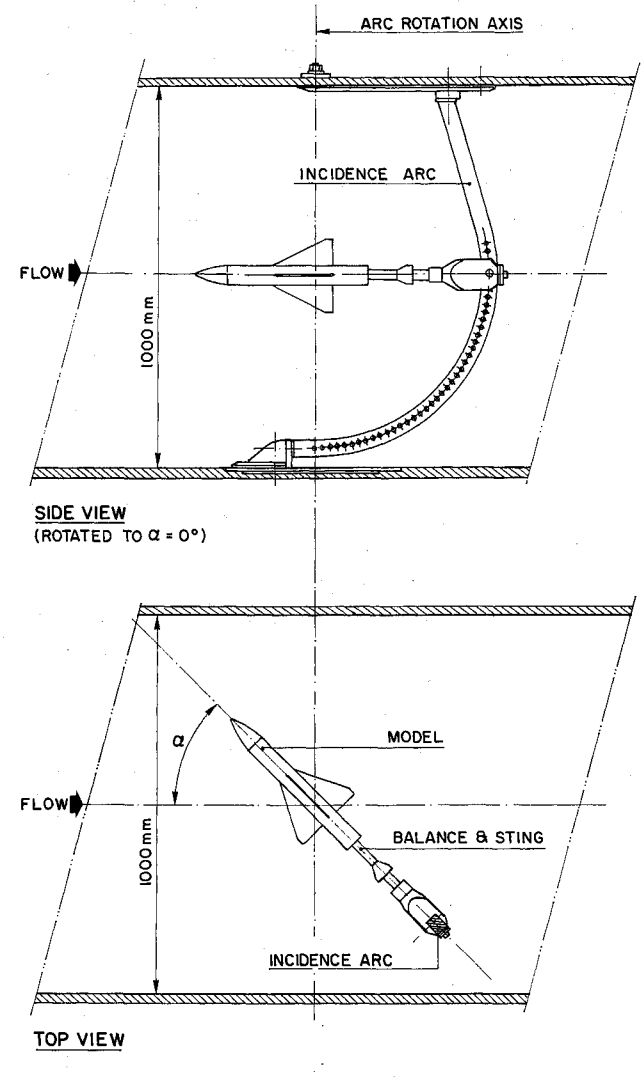

Fig. 2 Tunnel installation.

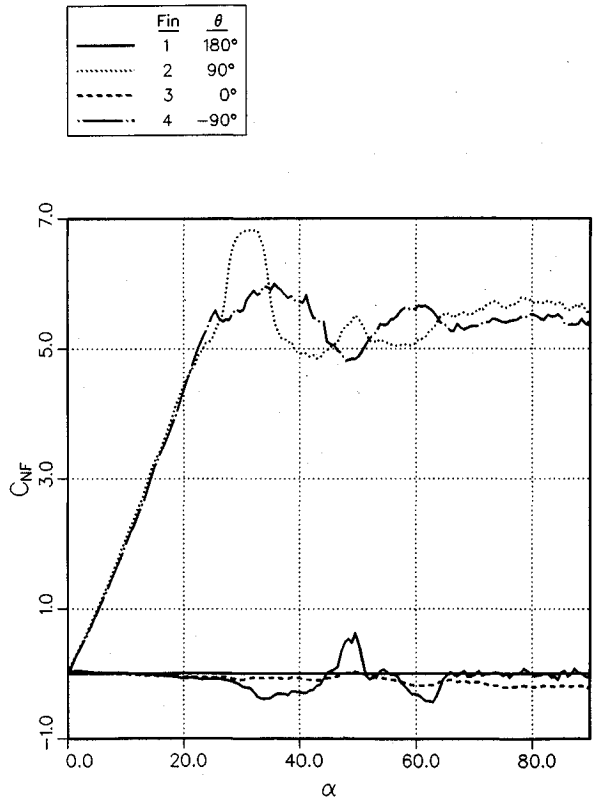

Fig. 3 Fin normal force coefficient at $\phi = 0$ deg for wing B at midposition.

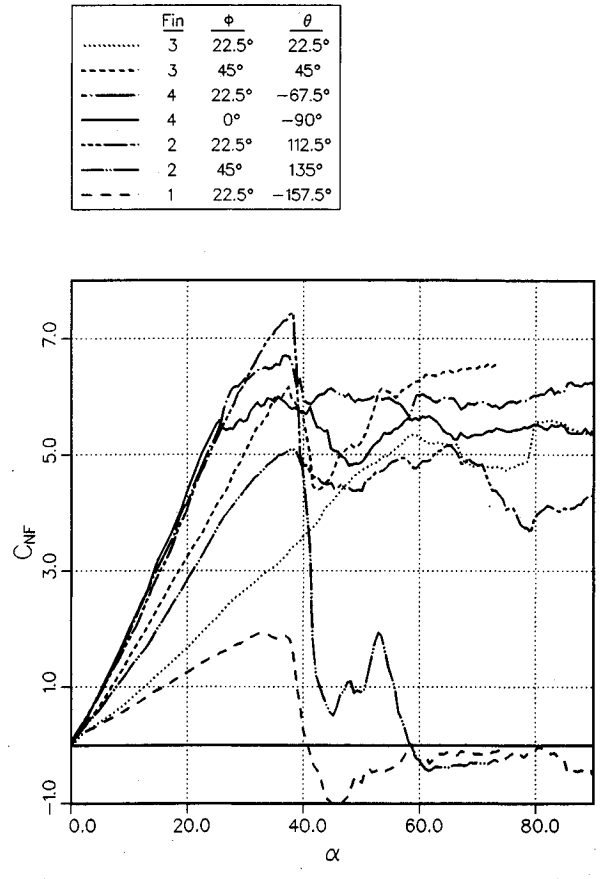

Fig. 4 Influence of the roll angle on the fin normal force coefficient for wing B at midposition.

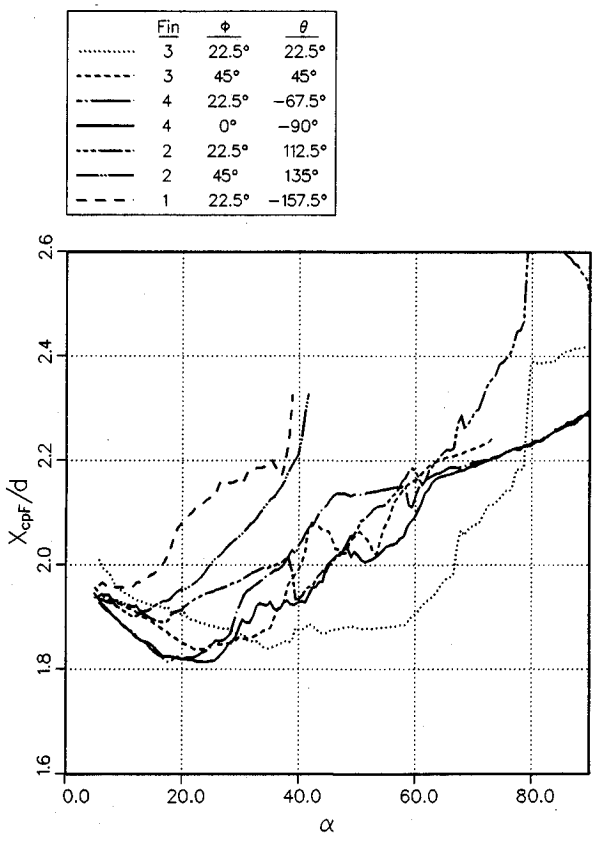

Fig. 5 Influence of the roll angle on the fin longitudinal center of pressure for wing B at midposition.

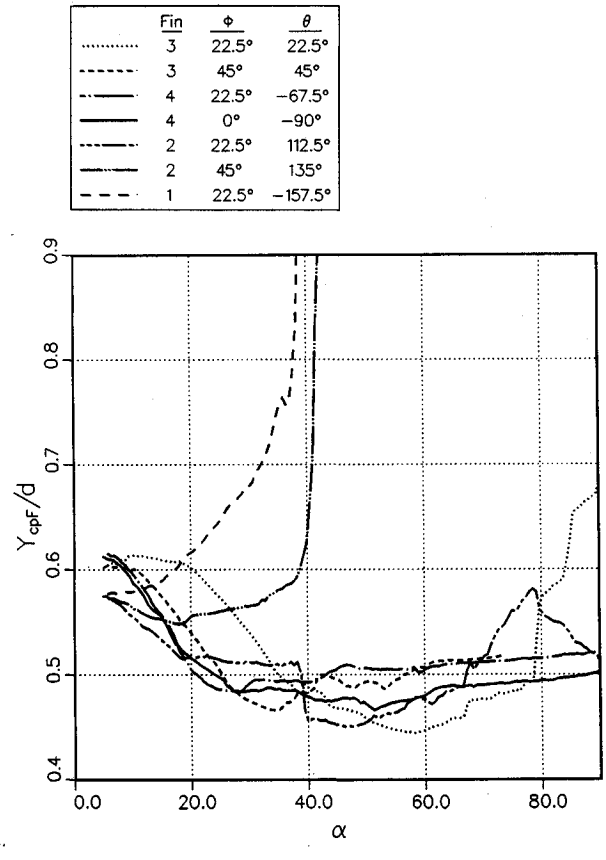

Fig. 6 Influence of the roll angle on the fin lateral center of pressure for wing B at midposition.

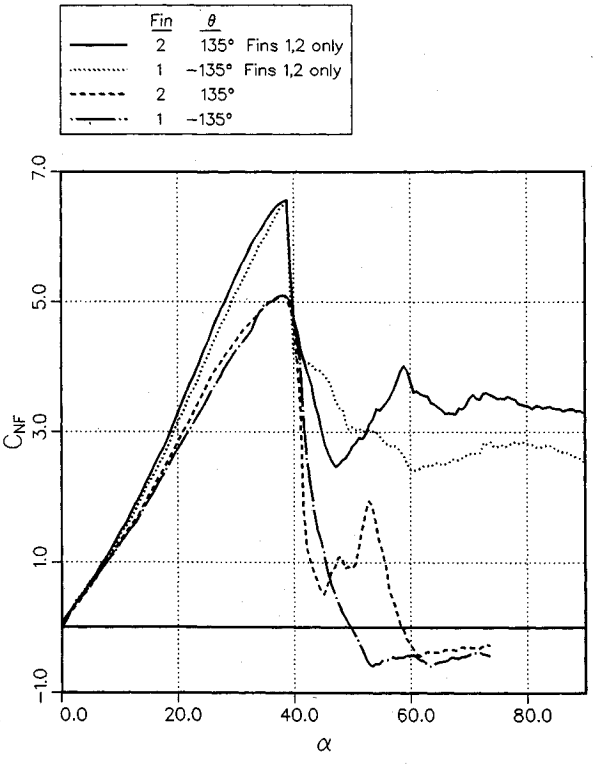

Fig. 7 Fin normal force coefficient on wing B at midposition and ϕ = 45 deg, with upper fins only.

At medium incidences ($25 < \alpha < 65$ deg), the normal force of the right fin (fin 4) is successively higher or lower than that of the left fin (fin 2) according to the model of Thomson and Morrison,[5] where new vortices are shed at the leeside of a body at high incidence, alternately at the left and right side. In this incidence range, a successively negative and positive normal force is measured on the upper fin (fin 1) as well as a difference in the longitudinal center of pressure of the horizontal fins, probably because of this alternate vortex shedding. This body influence is absent on a wing alone[13] and on the present wing-body configurations at $\alpha > 65$ deg.

When the wing-body configuration is set at a nonzero roll angle, the fin normal force coefficient C_{N_F} and the fin longitudinal and lateral centers of pressure X_{cp_F} and Y_{cp_F} are very significantly modified, as seen in Figs. 4–6 for wing B at midposition. At low incidences and for the lower fins ($|\theta| \leq 90$ deg), C_{N_F} increases according to the effective incidence on the fin, given by $\alpha.\sin|\theta|$, whereas a reduction in C_{N_F} is observed for the upper fins ($|\theta| \geq 90$ deg), and the center of pressure position depends only on the normal force, as already shown with the equivalent angle of attack concept.[15] At higher incidences, the dependence of the wing loads on α is presumably subject to two main events:

The wing vortex breakdown, present mainly at $|\theta| \leq 90$ deg, with a moderate decrease of C_{N_F} (this breakdown occurs at $\alpha \approx 60$ deg for ϕ = 11 and 22.5 deg and at $\alpha \approx 35$ deg for other azimuthal angles, as in the + attitude; after the breakdown, C_{N_F} remains generally constant with α, whereas its center of pressure moves backward, as in the + attitude).

The fin-to-fin interaction, present at $90 < |\theta| \leq 180$ deg, where the vortex breakdown on the lower fins possibly induces separated flow on the upper fins. A strong reduction occurs in C_{N_F}, and the center of pressure moves backward and outside. Also a strong correlation exists between upper and lower fins, for instance at ϕ = 45 deg and α = 40–60 deg, or at ϕ = 22.5 deg and α = 60–80 deg, between fins 3 and 2. It seems that at $|\theta| < 135$ deg, the flow is partially separated, whereas at $|\theta| \geq 135$ deg it is fully separated, and the fin normal force is reduced to zero.

Tests at ϕ = 45 deg with the upper fins only (fins 1 and 2, where $\theta = \pm 135$ deg), presented in Fig. 7, show that their normal force coefficient is partially reduced at $\alpha > 40$ deg, even in the absence of the lower fins, probably because of a body-wing interaction. On the other hand, no significant difference is observed on the lower fins C_{N_F} in the absence of the upper fins.

The fin normal force coefficient $C_{N_F}{}^*$, based on one fin planform area S^*, is plotted in Fig. 8 as a function of the azimuthal angle $|\theta|$, at different α, for the various tested configurations (wings A, B, and C at midposition and wing B at fore and back positions). At $\alpha \leq 30$ deg, $C_{N_F}{}^*$ is proportional to $\sin|\theta|$, with a minor reduction on the lee side. At higher incidences, $C_{N_F}{}^*$ is considerably reduced by the separated flow at high $|\theta|$, with a steep decrease at $|\theta| \geq 135$, 112.5, and 101 deg for α = 40, 60, and 80 deg, respectively. Also, the azimuthal angle for maximum $C_{N_F}{}^*$ decreases from $|\theta| = 90$ deg at $\alpha \leq 30$ deg to $|\theta| = 34$ deg at $\alpha \geq 70$ deg. Values of $C_{N_F}{}^*$ at $\alpha \approx 90$ deg and $|\theta| = 90$ deg are higher than the classical drag coefficient value of 1.2 on plates of similar aspect ratio in two-dimensional flow[13] because of the body influence. Such curves have been reported[4,15,16] for individual wing-body configurations at $\alpha \leq 40$ deg, with similar variation of C_{N_F} with the azimuthal angle. It is seen that the wing planform area and axial position have very little influence on the fin normal force coefficient, indicating no significant influence of the body vortices on the fin loads, except in the medium incidence range (Fig. 8b), and supporting the assumption on the fin-to-fin interaction.

Longitudinal Aerodynamic Characteristics

The overall wing contribution to the normal force coefficient, $C_{N_{W(B)}}$, and the body contribution to this coefficient, $C_{N_{B(W)}}$ are presented in Fig. 9 for wing B at midposition, at two roll angles, together with the body alone normal force C_{N_B}. The corresponding centers of pressure $X_{cp_{W(B)}}$, $X_{cp_{B(W)}}$, and X_{cp_B} are presented in Fig. 10. At ϕ = 0 deg, the wing contribution increases with up to the vortex breakdown, then after some decrease, it remains constant at $\alpha > 45$ deg, according to Fig. 4. The body contribution, on the other hand, increases continuously up to α = 70 deg, and is always greater than the body-alone normal force coefficient, which is typical of subcritical Reynolds numbers, with laminar separation.[7] As a result, the body contribution to the total normal force increases considerably with the angle of attack, from 29% at low to 59% at α = 70 deg. The wing contribution to the center of pressure is derived from Fig. 5, whereas the body contribution is near the body planform area.

These features emphasize a major difference between wings and bodies at high incidences.[17] For wings, there is a strong transition from axial flow to crossflow associated with the vortex breakdown, whereas for bodies, the transition is smooth. Also, for bodies, crossflow or impulsive flow analogies are good prediction tools up to very high incidences,[14,18] whereas simple predictive methods for wings, like Polhamus' analogy,[2] are effective only up to the vortex breakdown.[3]

When the wing-body configuration is set at a nonzero roll angle, the longitudinal aerodynamic characteristics are significantly modified. The sharp decrease in C_{N_F} at $\alpha > 40$ deg on the upper fins where $|\theta| \geq 135$ deg (Fig. 4) induces a decrease in the wing and the body contributions to the normal force coefficient, as seen in Fig. 9. As a result, the total normal force coefficient C_N is reduced by 20%, when the configuration is rolled from ϕ = 0 to 45 deg, between α = 40 and 80 deg, as shown in Fig. 11 for wing B at midposition. The normal force center of pressure X_{cp} (Fig. 12) moves forward as ϕ is increased because the body contribution becomes more important and is located at a more forward position than the wing contribution (Fig. 10). But at very high incidences ($\alpha > 80$ deg), at almost pure crossflow conditions, the influence of the roll angle tends to disappear for the normal force and its center of pressure.

The effects of the wing area and axial position on the normal force are presented in Fig. 13. The normal force coefficient is significantly increased when the wing area is increased, because of the wing contribution, and to a certain extent when the wing is moved backward, because of the increased body contribution. The body contributes up to 64 and 54% of the total normal force for wings A and C, respectively, at α = 70 deg and + attitude. At very

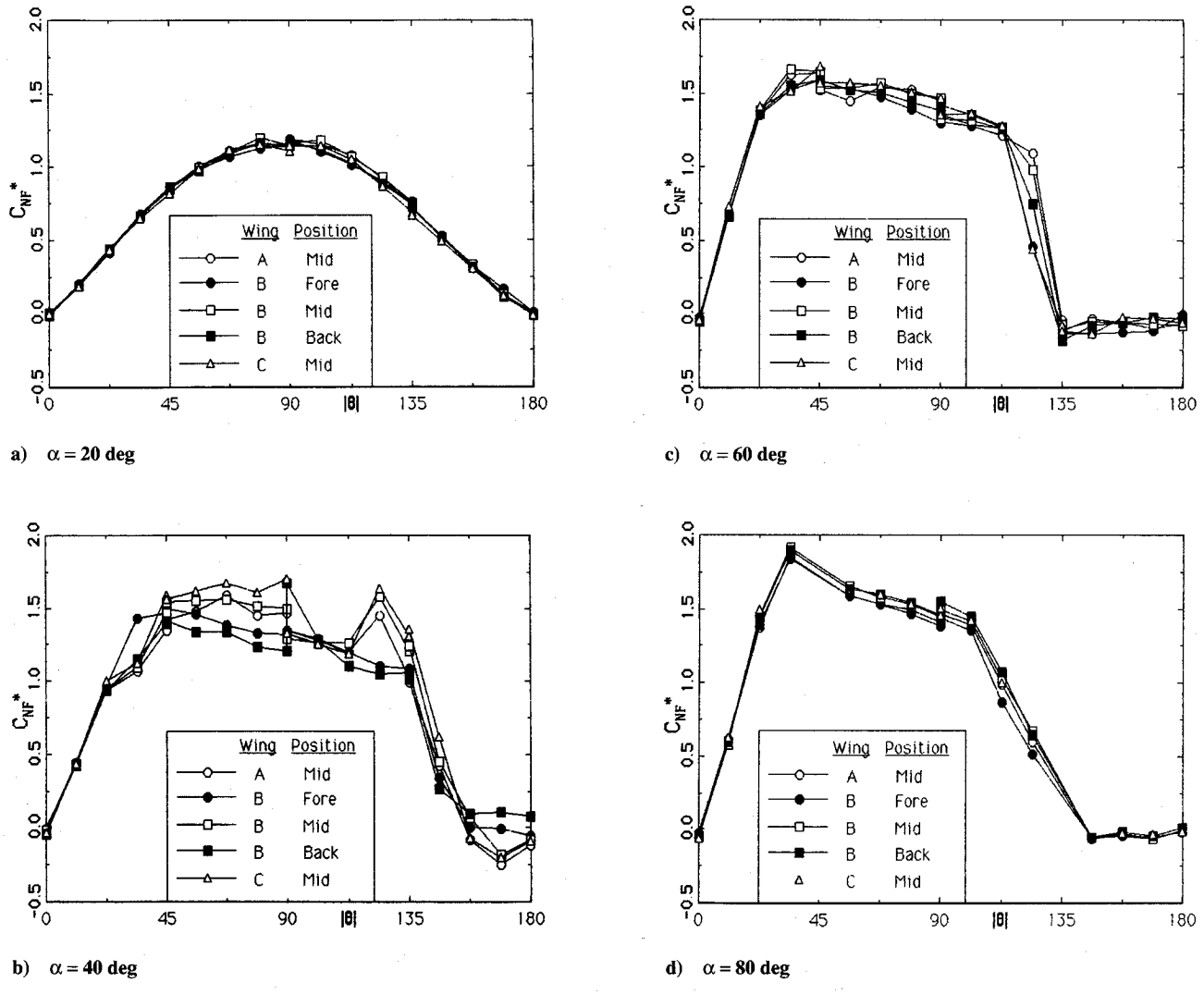

Fig. 8 Influence of the wing area and axial position on the fin normal force coefficient.

high incidences ($\alpha > 80$ deg), the center of pressure of the body contribution is independent of the wing area and position because of the almost pure crossflow conditions.

Rolling Moment

The rolling moment coefficient C_R is presented at five roll angles in Fig. 14, for wing B at midposition. At symmetrical + and × attitudes, asymmetric body vortices induce differential loads on the fins, as seen in Fig. 3 for the + attitude, which create a rolling moment. This successively positive and negative C_R is directly correlated to the successively positive and negative difference in the horizontal fins normal force in the + attitude, together with the upper fin contribution (Fig. 3). The differential loads as well as the rolling moment vanish at $\alpha > 65$ deg.

The range where this rolling moment is nonzero is typically $\alpha =$ 20–65 deg and is independent of the wing area and axial position, as shown in Fig. 15, where the rolling moment is plotted for the tested configurations at $\phi = 0$ deg. But its maximum value increases when the wing is moved backwards, because more and stronger vortices are shed on the lee side of the body, and when the wing area is increased, because of their increased influence on the wing fins.

At asymmetric roll angles, the sharp decrease of the upper fin normal force (Fig. 4) induces a strong rolling moment at $\alpha > 40$ deg (Fig. 14), because no moment is present to balance the rolling moment induced by the lower fin; C_R is larger at $\phi = 22.5$ and 34 deg than at $\phi = 11$ deg, because in that case the normal force on the lower fin is smaller (Fig. 4). Also, C_R is reduced at $\phi = 22.5$ and 34 deg between $\alpha = 60$ and 80 deg as a result of a local decrease in the fin 2 normal force (Fig. 4), because of the fin-to-fin interaction. This rolling moment does not vanish at very high incidences, as for symmetrical attitudes, because it is induced by separated flow on the fins, and not by the body vortices, and it is maximum at $\phi =$ 22.5 and 34 deg and $\alpha = 90$ deg.

This rolling moment coefficient is independent of the wing axial position but proportional to the wing planform area, as the fins' normal forces are (Fig. 8). This is shown in Fig. 16, where the rolling moment coefficient C_R^*, based on one fin planform area S^*, is plotted for the five tested configurations at $\phi = 22.5$ deg. It is seen that this coefficient is not significantly modified by changes in the wing area and axial position, except for two limited incidence regions. First, small variations in the wing vortex breakdown incidence for the different configurations induce a different evolution of C_R in the range $\alpha =$ 30–40 deg. Second, the influence of the asymmetrical body vortices in the range of $\alpha =$ 45–55 deg is observed in this rolling moment, as it was at symmetrical attitudes. A very similar dependence on α in the range $\alpha > 60$ deg is observed for the five configurations.

Lateral Aerodynamic Characteristics

The side force coefficient C_Y and the yawing moment coefficient C_n are presented at five roll angles in Figs. 17 and 18, for wing B at midposition. The wing and body contributions to these coefficients—$C_{Y_{W(B)}}$, $C_{Y_{B(W)}}$, $C_{n_{W(B)}}$, and $C_{n_{B(W)}}$—are presented in Figs. 19 and 20 for this configuration at $\phi = 0$ and 22.5 deg, together with the body-alone coefficients C_{Y_B} and C_{n_B}. Asymmet-

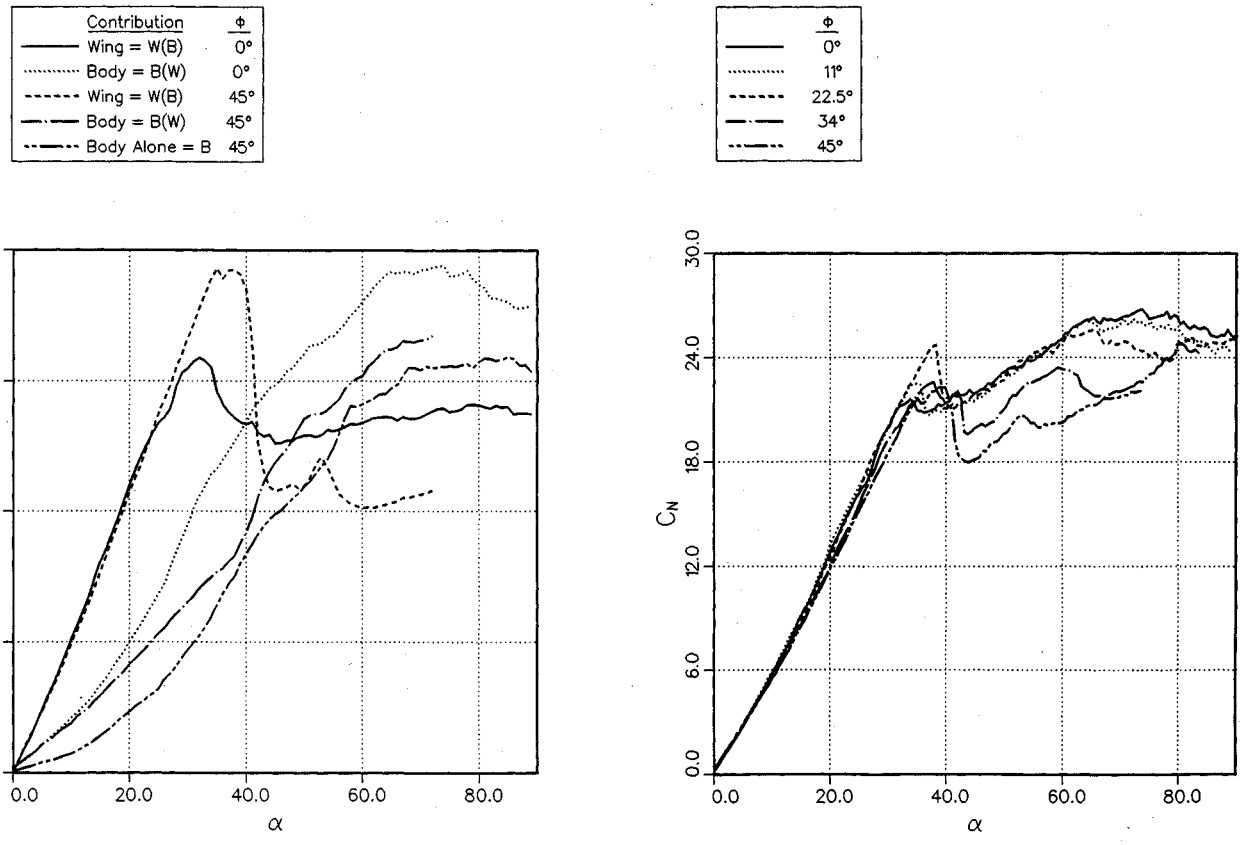

Fig. 9 Influence of the roll angle on the wing and body contributions to the normal force coefficient—wing B at midposition.

Fig. 11 Influence of the roll angle on the normal force coefficient—wing B at midposition.

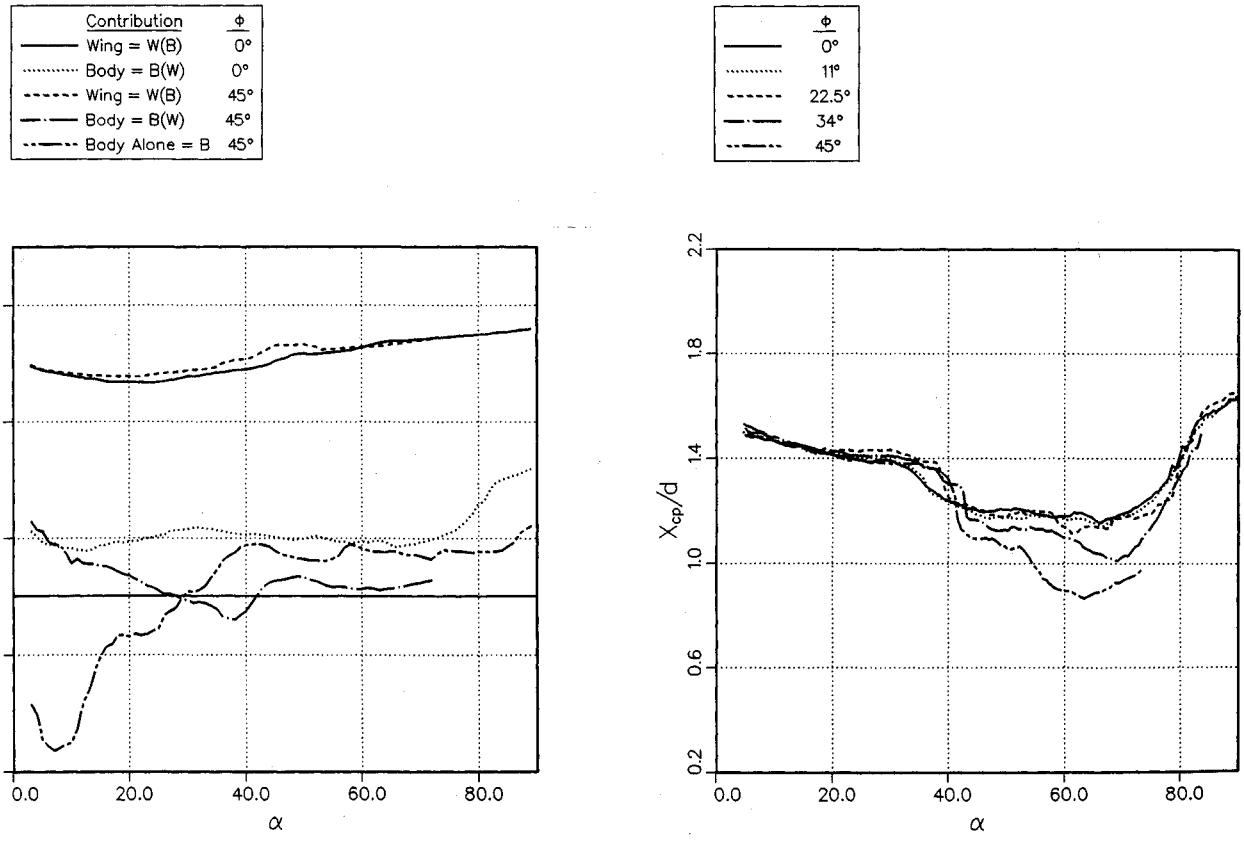

Fig. 10 Influence of the roll angle on the wing and body contributions to the longitudinal center of pressure—wing B at midposition.

Fig. 12 Influence of the roll angle on the longitudinal center of pressure—wing B at midposition.

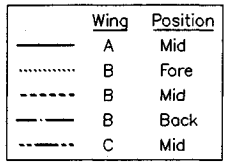

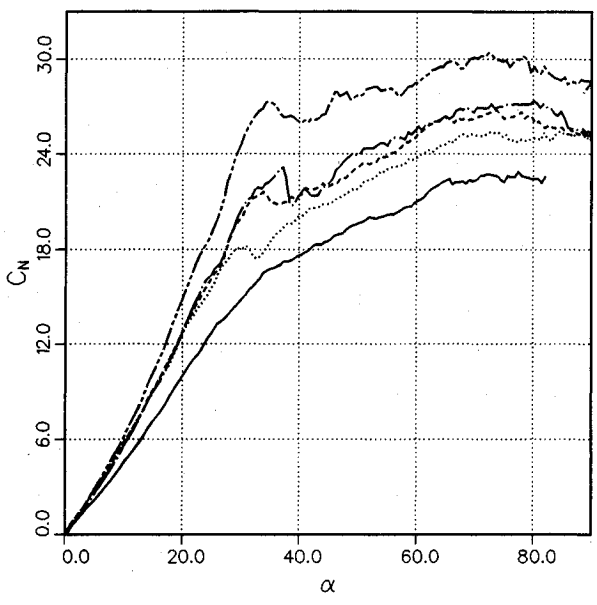

Fig. 13 Influence of the wing area and axial position on the normal force coefficient—$\phi = 0$ deg.

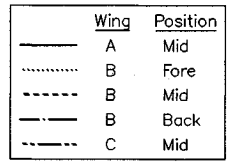

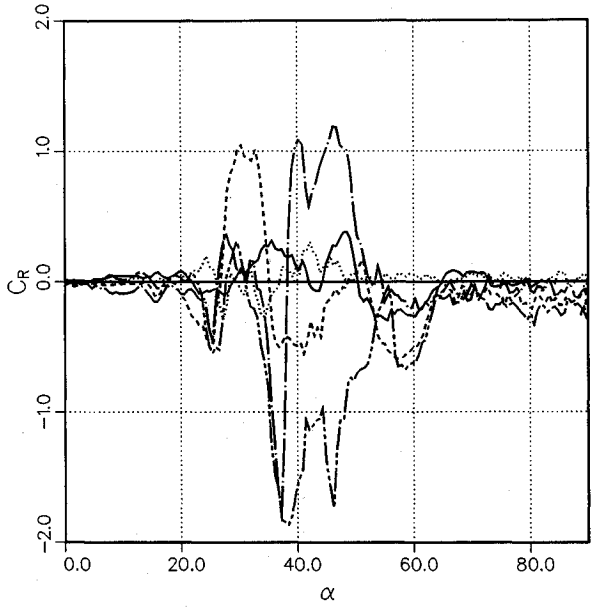

Fig. 15 Influence of the wing area and axial position on the rolling moment coefficient—$\phi = 0$ deg.

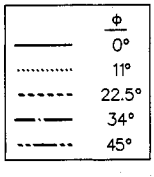

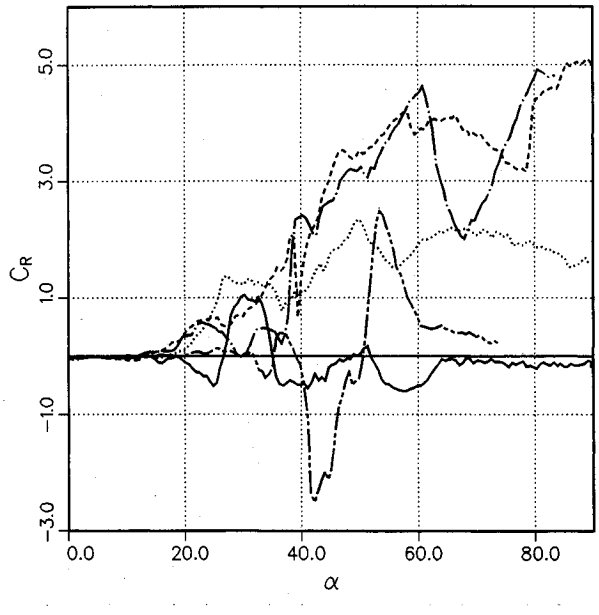

Fig. 14 Influence of the roll angle on the rolling moment coefficient—wing B at midposition.

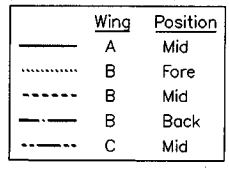

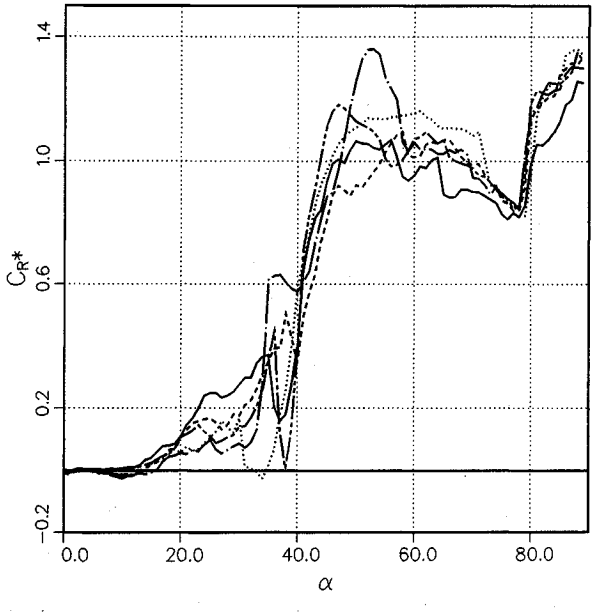

Fig. 16 Influence of the wing area and axial position on the rolling moment coefficient—$\phi = 22.5$ deg.

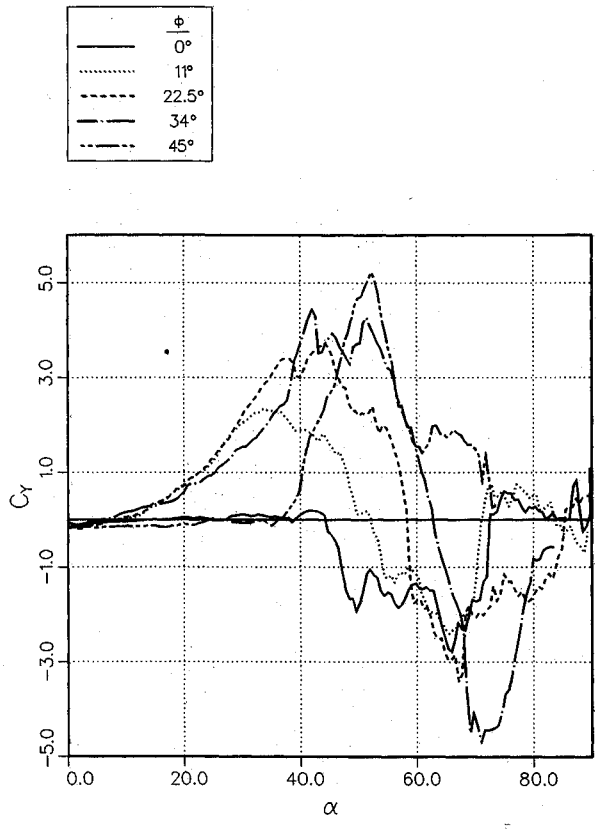

Fig. 17 Influence of the roll angle on the side force coefficient—wing B at midposition.

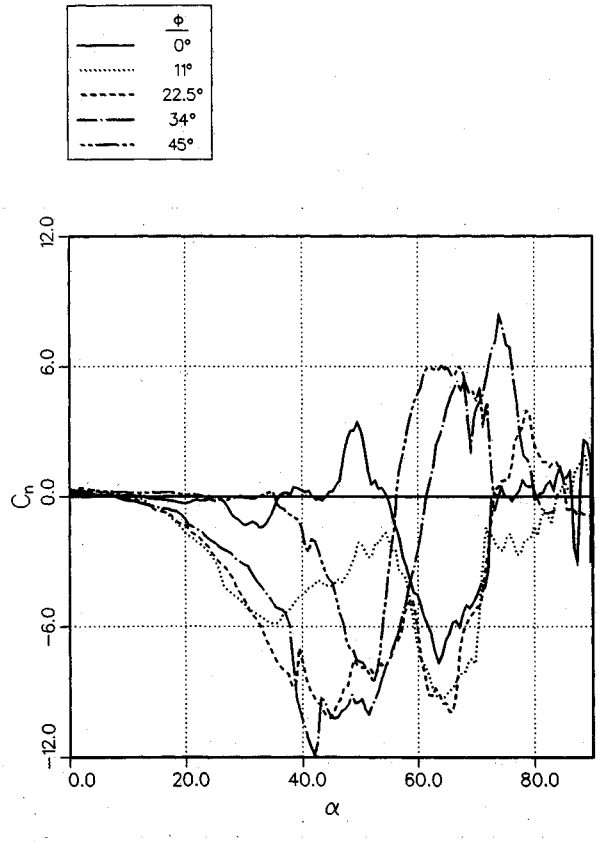

Fig. 18 Influence of the roll angle on the yawing moment coefficient—wing B at midposition.

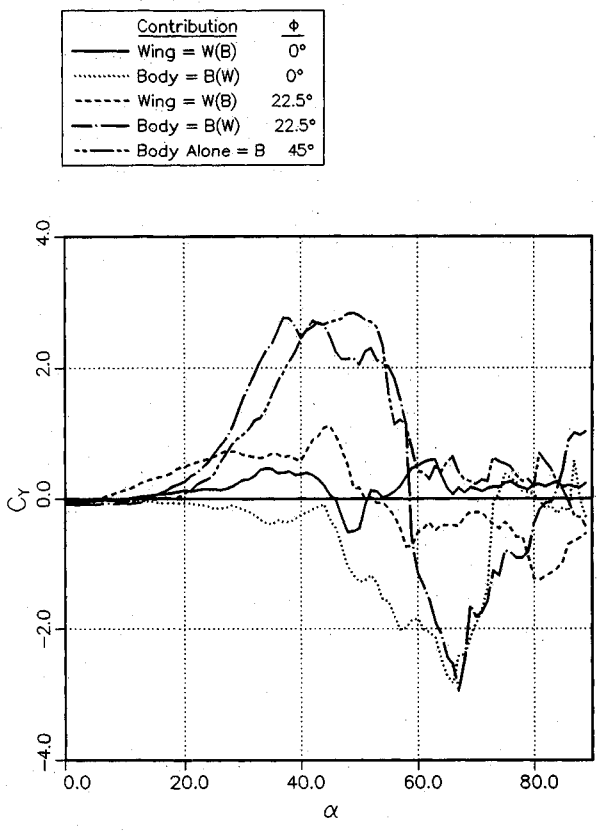

Fig. 19 Influence of the roll angle on the wing and body contributions to the side force coefficient—wing B at midposition.

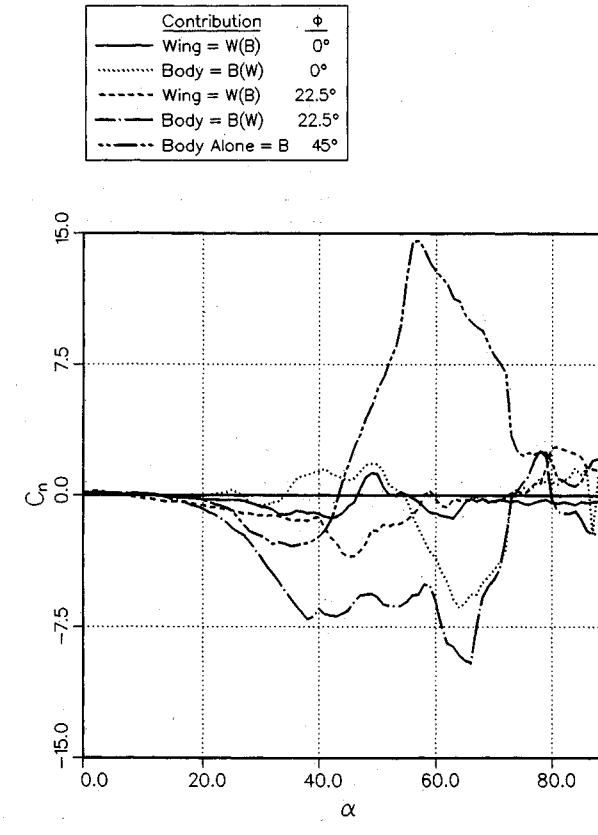

Fig. 20 Influence of the roll angle on the wing and body contributions to the yawing moment coefficient—wing B at midposition.

ric body vortices induce a side force and a yawing moment on the symmetrical configuration, as well as for the body alone. On the body alone, the side force appears at $\alpha = 20$ deg, and its center of pressure is located in the afterbody at $\alpha = 20$–30 deg (at about $7d$ from the body apex); C_Y increases up to 2.8 at $\alpha = 50$ deg, whereas its center of pressure moves forward, up to $1.5d$ from the body apex at $\alpha = 53$ deg. At $\alpha = 55$–75 deg, C_Y vanishes, but not C_n, indicating a pure yawing moment, probably because of a negative side force on the afterbody balancing the positive side force on the forebody. At $\alpha > 75$ deg, no significant C_Y or C_n are measured. This side force is also typical of subcritical Reynolds numbers, with laminar separation.[7] The onset angle for C_Y is in agreement with empirical predictions of Refs. 19 and 8, giving values of $\alpha = 22 \pm 5$ and 24 deg, respectively, for this body. Also, the magnitude and the angle of attack of the maximum side force are in agreement with the empirical predictions of Ref. 19, giving 3.6 ± 0.65 and 48 ± 7 deg, respectively.

Addition of wings at + and × attitudes delays the appearance of significant side force or yawing moment to $\alpha = 40$ deg (Figs. 17 and 18). For $\phi = 0$ deg, it is observed (Figs. 19 and 20) that the wing contribution to C_Y and C_n is small for all of the incidences. The body contribution is small up to $\alpha = 45$ deg; then it grows up to similar values to that of the body alone, but with a forebody center of pressure and no pure yawing moment in the range $\alpha = 55$–75 deg. It is concluded that the presence of symmetrical wings delays the onset of asymmetric body vortices on the afterbody at low and high incidences, but not on the forebody at $\alpha > 45$ deg. This feature is somewhat inverse to the influence of forebody strakes, which delays the formation of asymmetric vortices at the forebody but not at the afterbody, reducing C_Y at high angles of attack, but not at low α (Ref. 12).[12] The side force at × attitude is larger than at + attitude, as all of the fins contribute directly to C_Y.

At $\alpha > 65$ deg, asymmetric body vortices are disrupted, and the side force decreases progressively to zero at $\alpha = 75$ deg. The body contribution to the normal force decreases also in this crossflow region, and its center of pressure, as well as the total center of pressure, moves backward, as shown in Figs. 9, 10, and 12. It is also observed that at symmetric attitudes the rolling moment vanishes already at $\alpha > 65$ deg (Figs. 14 and 15), as well as the differential loads on the wing (Fig. 3). It is suggested that in the range $\alpha = 65$–75 deg decreasing asymmetrical body vortices still induce a side force on the forebody but cease to induce differential loads on the wing.

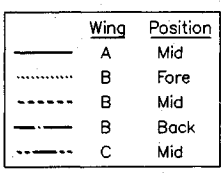

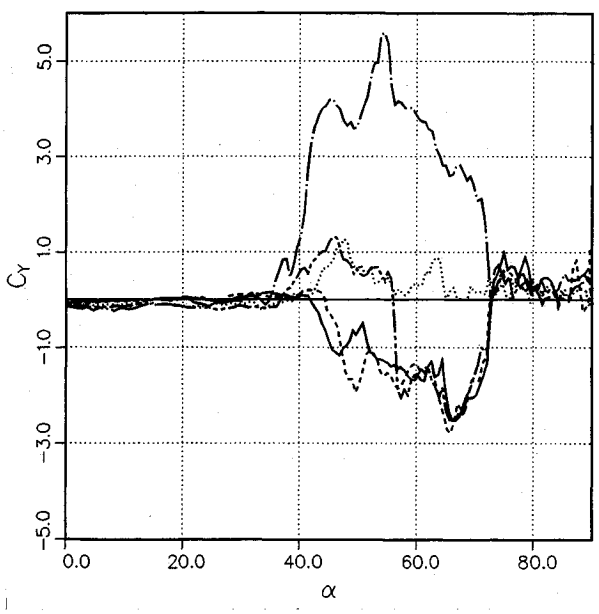

Fig. 21 Influence of the wing area and axial position on the side force coefficient—$\phi = 0$ deg.

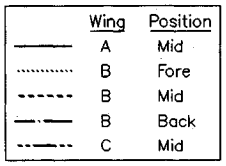

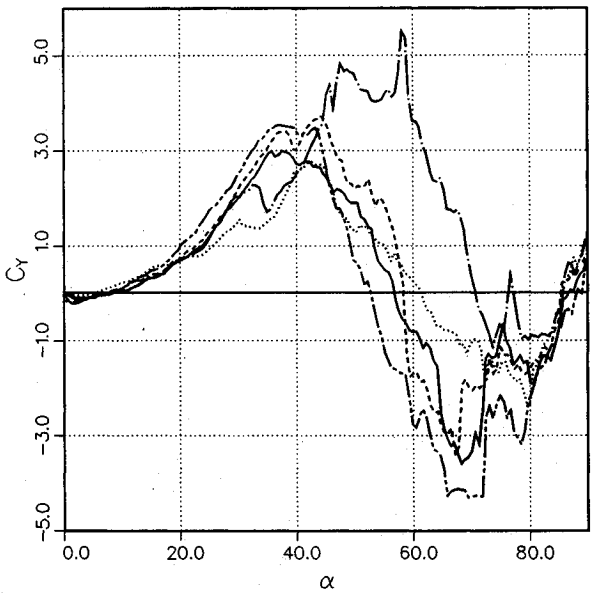

Fig. 22 Influence of the wing area and axial position on the side force coefficient—$\phi = 22.5$ deg.

The range where C_Y or C_n are nonzero is typically $\alpha = 40$–75 deg for symmetrical attitudes and is independent of the wing area and axial position, as shown in Fig. 21, where C_Y is plotted for the tested configurations at $\phi = 0$ deg. The maximum side force value increases when the wing is moved backward, as for the rolling moment, but is independent of the wing area, because the wing contribution to the side force is very low compared with the body contribution. As a matter of fact, the curves of C_Y are very repetitive for the three wings at the midposition. The side force center of pressure is located in the wing section at $\alpha < 55$ deg, and then it moves to the forebody section.

At asymmetric positive roll angles, the nonlinear component of the fin normal force induces a positive side force, already at $\alpha > 5$ deg, theoretically proportional to $(\cos^2\phi.\sin\phi - \sin^2\phi.\cos\phi)$. But above $\alpha = 30$ deg, the main contribution to the side force is the body, as shown in Fig. 19. At $\alpha < 55$ deg, the body contribution is similar to the side force of the body alone, but at $\alpha > 55$ deg, it is similar to the body contribution at $\phi = 0$ deg. It seems that, contrary to the + attitude, the presence of wings reduces the asymmetric body vortices on the afterbody at high angles of attack (giving C_Y with a forward center of pressure), whereas it does not reduce these vortices at low incidences (giving C_Y with a backward center of pressure). As a result of the major body contribution, the maximum side force is not higher than at the + and × attitudes, and the side force center of pressure is almost independent of the roll angle. Also, the side force is rather independent of the wing area but increases when the wing is moved backward, as for the + attitude, as shown in Fig. 22, for the different configurations at $\phi = 22.5$ deg.

Conclusions

1) The roll angle affects significantly the fin normal force coefficient on a cruciform wing-body configuration at high incidences. The normal force on the upper fins decreases to zero, at $\alpha > 40$ deg and $|\theta| > 135$ deg, possibly because the vortex breakdown on the lower fins induces separated flow over the upper fins. As a result, a strong rolling moment is induced at these incidences at asymmetric roll angles, being maximum at $\phi = 22.5$ deg and $\alpha = 90$ deg. This rolling moment is much larger than the rolling moment induced on symmetrical configurations by the asymmetric body vortices and does not vanish at very high incidences.

2) The wing contribution to the side force is small compared with the body contribution at asymmetric roll angles. As a result, the maximum side force is not higher than that obtained at symmetric + and × attitudes, but side forces are measured at all incidences. The roll angle also affects the normal force, which is reduced as ϕ is increased for $\alpha > 40$ deg, and its center of pressure, which moves forward, as the body contribution becomes more important.

3) Moving the wing backward does not affect the fin normal force coefficient, but more and stronger vortices are shed on the leeside of the body. As a result, larger normal forces and larger side forces are measured on symmetric and asymmetric configurations as the wing is moved backward, as well as larger rolling moments at symmetric attitudes. However, the rolling moment on asymmetric configurations remains unaltered, as it is induced by the fins' normal force. The influence of the asymmetric body vortices is noticeable only at medium incidences.

4) When the wing area is increased with a constant span, the fin normal force coefficient C_{N_F} gets larger, according to the area increase, but the normal force coefficient $C_{N_F}{}^*$, based on the fin area, remains unaltered. As a consequence, the total normal force is significantly increased. The rolling moment at asymmetric roll angles is proportional to the wing planform area, and the rolling moment coefficient $C_R{}^*$, based on the fin area, remains unchanged. The body vortices are not significantly modified when the wing area is increased, but their influence on the wing is enhanced. As a result, the maximum side force is unchanged, whereas the maximum rolling moment on symmetric configurations is increased.

Acknowledgment

This research was supported by the Kurt Haber Applied Aerospace Research Fund.

References

[1]Howard, R. M., Rabang, M. P., and Roane, D. P., Jr., "Aerodynamic Effects of a Turbulent Flowfield in a Vertically Launched Missile," *Journal of Spacecraft and Rockets,* Vol. 26, No. 6, 1989, pp. 445–451.

[2]Polhamus, E. C., "A Concept of the Vortex Lift of Sharp-Edge Delta Wings Based on a Leading-Edge-Suction Analogy," NASA TN D-3767, Dec. 1966.

[3]Wentz, W. H., Jr., and Kohlman, D. L., "Vortex Breakdown on Slender Sharp-Edged Wings," *Journal of Aircraft,* Vol. 8, No. 3, 1971, pp. 156–161.

[4]Nielsen, J. N.,"Nonlinearities in Missile Aerodynamics," AIAA Paper 78-20, Jan. 1978.

[5]Thomson, K. D., and Morrison, D. F., "The Spacing, Position and Strength of Vortices in the Wake of Slender Cylindrical Bodies at Large Incidence," *Journal of Fluid Mechanics,* Vol. 50, Pt. 4, 1971, pp. 751–783.

[6]Lamont, P. J., and Hunt, B. L.,"Pressure and Force Distributions on a Sharped–Nosed Circular Cylinder at Large Angles of Inclination to a Uniform Subsonic Stream," *Journal of Fluid Mechanics,* Vol. 76, Pt. 3, 1976, pp. 519–559.

[7]Lamont, P. J., "Pressures Around an Inclined Ogive Cylinder with Laminar, Transitional or Turbulent Separation," *AIAA Journal,* Vol. 20, No. 11, 1982, pp. 1492–1499.

[8]Ericsson, L. E., and Reding, J. P., "Asymmetric Vortex Shedding from Bodies of Revolution," *Tactical Missile Aerodynamics,* edited by M. J. Hemsch, and J. N. Nielsen, Vol. 104, Progress in Astronautics and Aeronautics, AIAA, New York, 1986, pp. 243–296.

[9]Clark, W. H., Peoples, J. R., and Briggs, M. M., "Occurrence and Inhibition of Large Yawing Moments During High–Incidence Flight of Slender Missile Configurations," *Journal of Spacecraft and Rockets,* Vol. 10, No. 8, 1973, pp. 510–519.

[10]Ericsson, L. E., and Reding, J. P., "Alleviation of Vortex–Induced Asymmetric Loads," *Journal of Spacecraft and Rockets,* Vol. 17, No. 6, 1980, pp. 546–553.

[11]Modi, V. J., Cheng, C. W., Mak, A., and Yokomizo, T.,"Reduction of the Side Force on Pointed Forebodies Through Add–On Tip Devices," AIAA Paper 90-3005, Aug. 1990.

[12]Yuan, C.-C., and Howard, R. M., "Effects of Forebody Strakes on Asymmetric Vortices for a Vertically-Launched Missile," *Journal of Spacecraft and Rockets,* Vol. 28, No. 4, 1991, pp. 411–417.

[13]Hoerner, S. F., *Fluid–Dynamic Drag,* Hoerner Fluid Dynamics, Brick Town, NJ, 1965, pp. 3–16.

[14]Jorgensen, L. H., "Prediction of Static Aerodynamic Characteristics for Slender Bodies Alone and with Lifting Surfaces to Very High Angles of Attack," NASA TR R-474, Sept. 1977.

[15]Hemsch, M. J., and Nielsen, J. N., "Equivalent Angle-of-Attack Method for Estimating Nonlinear Aerodynamics of Missile Fins," *Journal of Spacecraft and Rockets,* Vol. 20, No. 4, 1983, pp. 356–362.

[16]Perinelle, J., and Lupieri, A., "Présentation d'un Bassin Hydrodynamique," AGARD-CP-413, Oct. 1986.

[17]Hemsch, M. J., "Component Build-Up Method for Engineering Analysis of Missiles at Low-to-High Angles of Attack," *Tactical Missile Aerodynamics: Prediction Methodology,* edited by M. R. Mendenhall, Vol. 142, Progress in Astronautics and Aeronautics, AIAA, Washington, DC, 1992, pp. 115–169.

[18]Thomson, K. D.,"The Estimation of Viscous Normal Force, Pitching Moment, Side Force and Yawing Moment on Bodies of Revolution at Incidences up to 90°," Australian Weapons Research Establishment, W.R.E. 782, Salisbury, England, UK, Oct. 1972.

[19]Wardlaw, A. B., Jr., and Morrison, A. M., "Induced Side Forces at High Angles of Attack," *Journal of Spacecraft and Rockets,* Vol. 13, No. 10, 1976, pp. 589–593.

Jerry M. Allen
Associate Editor